DOI: 10.15669/pnst.4.337

Progress in Nuclear Science and Technology
Volume 4 (2014) pp. 337-340

ARTICLE

Activation detector measurements at the hadron absorber of the NuMI neutrino beamline at Fermilab

Norihiro Matsuda[a*], Yoshimi Kasugai[a], Hiroshi Matsumura[b], Hiroshi Iwase[b], Akihiro Toyoda[b], Hiroshi Yashima[c], Shun Sekimoto[c], Koji Oishi[d], Yukio Sakamoto[e], Hiroshi Nakashima[a], Takashi Nakamura[f], David Boehnlein[g], Gary Lauten[g], Anthony Leveling[g], Nikolai Mokhov[g] and Kamran Vaziri[g]

[a]Japan Atomic Energy Agency, 2-4 Shirakata-Shirane, Tokai-mura, Naka-gun, Ibaraki, 319-1195, Japan; [b]High Energy Accelerator Research Organization (KEK), 1-1 Oho, Tsukuba, Ibaraki, 305-0801, Japan; [c]Kyoto University Research Reactor Institute, Kumatori-cho, Sennan-gun, Osaka, 590-0494, Japan; [d]Shimizu Corporation, 4-17, Etchujima 3-chome, Koto-ku, Tokyo, 135-8530, Japan; [e]ATOX Co. Ltd, Technical Development Center, 1201 Takada, Kashiwa, Chiba, 277-0861, Japan; [f]Tohoku University, Aoba, Aramaki, Aoba-ku, Sendai, Miyagi, 980-8578, Japan; [g]Fermi National Accelerator Laboratory, Batavia, IL, 60510, USA

Two-dimensional distributions of the production rates of radionuclides in aluminum and gold activation detectors, placed behind the hadron absorber of the NuMI beamline at Fermilab were obtained in an experiment for shielding data as a dump in a proton-beam-energy domain above 100 GeV. The production rates of ^{7}Be, ^{22}Na, and ^{24}Na in the aluminum activation detectors and those of ^{185}Os, ^{194}Au, and ^{196}Au in the gold activation detectors were obtained from the γ-ray spectra of HPGe counters. It was concluded that in these distributions showed some peaks that can be attributed to a lack of shielding caused by the gaps for arraignment and cooling in the hadron absorber. The radionuclides in the activation detectors were mainly produced by neutrons, protons and pions, according to analyses of calculated results by the PHITS code.

Keywords: high energy accelerator; shielding experiment; secondary particles; activation method

1. Introduction

The Japanese-American Study of Muon Interaction and Neutron Detection (JASMIN) is a collaboration that undertakes experimental studies of shielding and radiation effects for high-energy accelerators at the Fermi National Accelerator Laboratory (Fermilab) [1]. One of the purposes is to acquire of shielding data in a proton beam energy region above 100 GeV.

Inter-comparisons for neutron attenuation length among simulation codes have been performed by Hirayama et al. as one of the activities of the task force on Shielding Aspects of Accelerators, Targets and Irradiation Facilities (SATIF). The source condition of the simulation problem is mono-energetic parallel beam, and the geometry is infinite plane of iron or concrete, respectively. Since SATIF-7 [2], some discrepancies have been observed in the energy region above a few GeV. The differences caused by the increasing energy were mainly due to secondary mesons produced in the shield. However, although an experiment under ideal conditions such as the inter-comparison cannot be performed to confirm this attenuation phenomenon, a few shielding experiments at more than 1 GeV have been conducted so far [3, 4]. Further experimental data are strongly needed, especially in a proton-beam-energy region above a few tens of GeV.

The Neutrino at the Main Injector (NuMI) beamline at Fermilab was designed to provide an intense muon-neutrino to research the phenomena of neutrino mixing and oscillation [5]. The NuMI has a graphite target with a set of magnetic horns producing π mesons. Protons of 120 GeV/c are delivered from the Fermilab main injector at an average power of up to 400 kW. The mesons travel through a decay pipe, where neutrinos and muons are produced via π decay. A hadron absorber is present at the end of the decay pipe, which serves as a dump, to absorb primary protons, which do not interact in the neutrino target, secondary hadrons, and undecayed mesons. The hadron absorber consists of a pile of aluminum, iron, and concrete. It is interesting to note that a number of neutrinos and accompanying muons easily pass through the hadron absorber depending on the penetrating power. Therefore, the area behind the hadron absorber in the absorber enclosure will hopefully serve as an intense muon field. The distance from the neutrino target to the hadron absorber, that is, the length of the decay pipe, is 675 m. The remaining protons are thought to be a parallel beam collimated by the concrete shield covering the decay pipe. Therefore, the area around the hadron absorber has appropriate conditions for verifying the attenuation length for the SATIF problem.

*Corresponding author. Email: matsuda.norihiro@jaea.go.jp

In this study, two-dimensional distributions of the production rate of radionuclides produced in activation detectors placed behind the hadron absorber were obtained in an experiment for shielding data as a dump using 190 sets of aluminum and gold activation detectors. The distributions with some peaks were compared with calculations using the PHITS [6] code.

2. Experiment

Figure 1 shows a cross-sectional view around the absorber enclosure of the NuMI. Almost all remaining primary protons, and secondary hadrons produced from the neutrino target are absorbed by the hadron absorber. The hadron absorber consists of the absorber core and many shielding blocks. The absorber core is constructed from aluminum and iron plates. The total thicknesses of the aluminum and iron plates with 244 and 231 cm, respectively. The absorber core is surrounded by iron and concrete blocks. The back side of the core is composed of some concrete blocks that have a thickness of 91.4 cm.

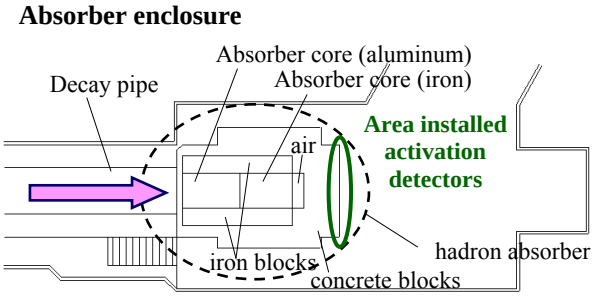

Figure 1. Cross-sectional view of the absorber enclosure of the NuMI. Shielding materials are aluminum, iron, and concrete with thicknesses of 244, 231, and 91.4 cm, respectively.

A total of 190 sets of activation detectors, pure aluminum (chemical purity: 99.99%) and gold foil (chemical purity: 99.95%), were installed at regular intervals at the back surface of the concrete block as shown in Figure 1, to cover the core. The sizes of the aluminum and gold foil were 20 mmφ × 5 mm^{t} and 10 mm × 10 mm × 0.1 mm^{t}, respectively. The cross-sectional size of the measurement area and the core plate were 200 × 200 cm^2 and 129.5 × 129.5 cm^2, respectively, as shown in **Figure 2**. There were some holes in the core plate at the top and on both sides for arraignment and cooling, with corresponding diameters of 5.7 and 3.7 cm, respectively.

The irradiation for the experiment lasted 128.7 days. After the irradiation, γ-rays emitted from the activation detectors were measured with high-purity germanium (HPGe) detectors. The nuclear data of the radionuclides used for the activation detectors are listed in **Table 1** [7]. During the experiment, an average of 1.30 × 10^{13} protons/s was delivered from the main injector to the neutrino target, placed very far upstream from the absorber enclosure. Protons, which passed through the target without interaction, were estimated to be 1.08 × 10^{12} protons/s based on a calculation result by MARS15 [8] code.

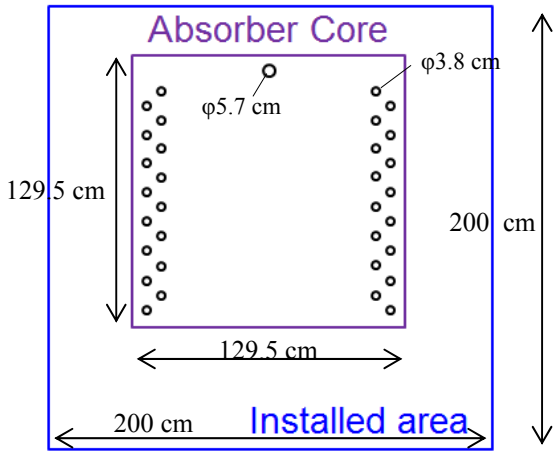

Figure 2. Cross-sectional view of the size of the absorber core with one arraignment hole and 32 cooling holes, which are 5.7 and 3.8 cm, respectively, and the installed area of the activation detectors.

The production rates of the radionuclides were determined after being corrected for the peak efficiency of the HPGe detectors and the beam current fluctuation during irradiation. One of the HPGe detectors had been calibrated by Canberra, and the peak efficiency was determined using Canberra's LabSOCS software [9]. For the other detectors, the peak efficiencies were determined on the basis of the ratios of their peak counting rates to those of the peak counting rates of the calibrated detector. The components of estimated errors in the production rates were the counting statistics and the detector efficiency.

Table 1. Nuclear properties of the radionuclides.

Activation detector	Product nuclide	Half-life	Gamma-ray energy(keV)	Branching ratio (%)
Al	^{7}Be	53.29 d	477.595	10.52
Al	^{22}Na	2.6019 y	1274.53	99.944
Al	^{24}Na	14.9590 h	1368.633	100
Au	^{185}Os	93.6 d	646.116	78
Au	^{194}Au	38.02 h	328.50	60
Au	^{196}Au	6.183 d	355.68	86.9

3. Results and discussion

Figure 3 shows a two-dimensional distribution of the production rate of ^{7}Be produced in the aluminum activation detectors. The numerical values of the production rate indicated a color contour figure from white (minimum value = maximum value × 1/100) to dark red (maximum value: 1.8 × 10^{-34} target nucleus^{-1} proton^{-1}), except for an affected white region at the bottom left in the absorber core where no data were collected. The cross-sectional shape of the core and the diameter of the decay pipe extended by the gradient (3.3 degrees) of the beamline are also indicated in the figure,

with purple square and black solid oval lines, respectively. The extension caused by the thickness of the hadron absorber is 35.3 cm. The figure has a large double peak on the right and left edges of the absorber core and a small peak on the top of the core. All the nuclides in Table 1 showed a tendency similar to that of the color contour figure. The large peaks appeared within the 182.9 cm diameter of the decay pipe as indicated by the solid black line. Also, the area of the peak on the whole fits in the gaps of the absorber core. The peak area spreads toward the outside of the absorber core because the thickness of the side plates that are wedged between the absorber core and the surrounding shield is lesser than the core thickness.

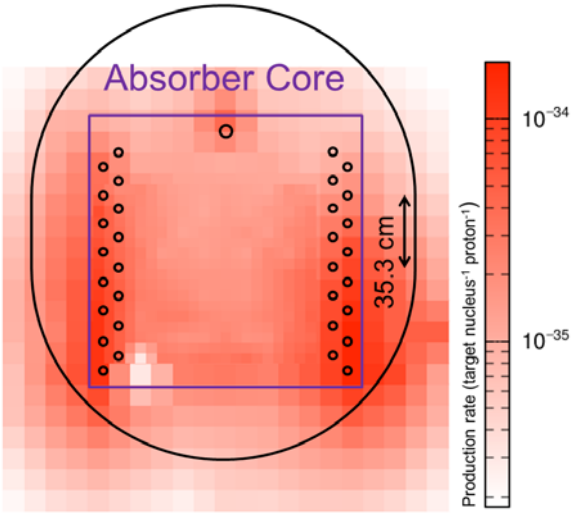

Figure 3. Two-dimensional distribution of the production rate of ^{7}Be produced in the aluminum activation detectors. The maximum value (dark red) is 1.8 × 10^{-34} target nucleus^{-1} proton^{-1}, and the minimum value (white) is the maximum value × 1/100. The solid purple line indicates the size of the absorber core. The solid black line is the 182.9-cm-diameter line that is considered as the gradient of the beamline. The diameter of the decay pipe is 182.9 cm.

The next focus is on horizontal distributions of the production rate of radionuclides produced in the activation detectors. At the vertical center of the absorber core, the horizontal distributions of the production rates of ^{7}Be, ^{22}Na, and ^{24}Na in the aluminum activation detectors are shown in **Figure 4**. The production rates of ^{194}Au, ^{196}Au, and ^{185}Os in the gold activation detectors are shown in **Figure 5**. The positions of both peaks in the horizontal distributions of the production rate showed good agreement among the radionuclides produced. The profile of the production rate distribution showed line symmetry at the center of the decay pipe. The production rates at the peak position were 2-5 times higher than those at the horizontal center (X-position in the figures is 0 cm). Further, the values around 0 cm were nearly flat. If the beam have spatial intensity distribution, these production rates distributions around the center might not become flat. As shown in Figures 4 and 5, the heavier the nuclide, the broader the distribution. The types of nuclides produced in the activation detectors are related to the energy of the particles in the field. Thus, the gaps in the absorber core exist only up to the core end, and the distributions of each peak configured by low-energy particles are broadened by the following concrete blocks behind the core.

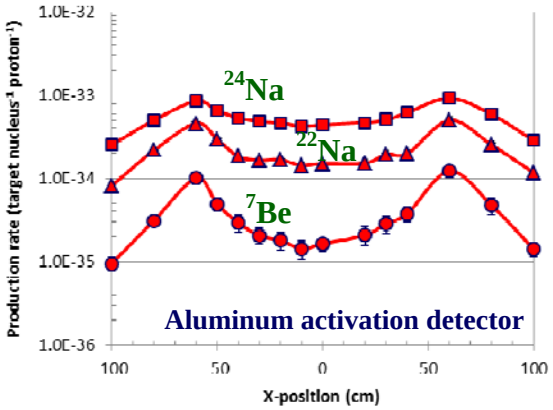

Figure 4. Horizontal distributions of the production rates of ^{7}Be, ^{22}Na, and ^{24}Na in the aluminum activation detectors.

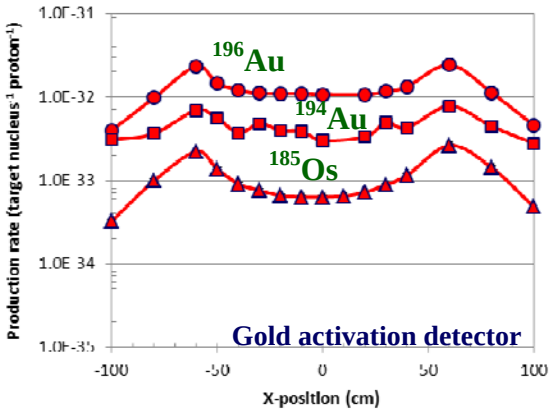

Figure 5. Horizontal distributions of the production rates of ^{194}Au, ^{196}Au, and ^{185}Os in the gold activation detectors.

Calculation analyses for production rates were performed with the PHITS code. In the calculation, it was assumed that particles were bombarded perpendicularly on the surface of the hadron absorber. Here secondary neutron, proton, pion^{+}, and pion^{-} were considered inducible particles. Arrival factors of the particles bombarded on the surface of the hadron absorber were estimated by calculating the particle transport from the neutrino target to the hadron absorber with MARS15. In this condition, at the beam center, the calculation results for the production rates of ^{7}Be, ^{22}Na, and ^{24}Na in the aluminum detectors and ^{185}Os, ^{194}Au, and ^{196}Au in the gold detectors were in agreement with the experimental data within a factor of 5. C/E values of each are shown in **Figure 6**. In case of the reaction rate of ^{24}Na having a low threshold energy, although the values are lower, the difference is likely due to covering to add immediate constructions within the calculation geometry and so on. However, in case of the production rate of ^{185}Os, a new model or new calculation process using a heavier target may be needed to calculate

multi-fragmentation of the compound nucleus with high energy. From the C/E results in Figure 6, we found that the analysis will be sufficient to consider the productions by neutrons, protons and pions.

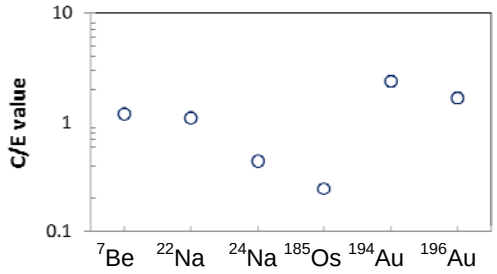

Figure 6. C/E values of the production rates of ^{7}Be, ^{22}Na, and ^{24}Na in the aluminum activation detector, and those of ^{185}Os, ^{194}Au, and ^{196}Au in the gold activation detector at the beam center.

By the PHITS calculation, the attributable fractions of secondary neutron, proton, pion^{+}, and pion^{-} were 29%, 16%, 30%, and 25% for ^{7}Be; 70%, 10%, 8%, and 12% for ^{22}Na; and 87%, 4%, 3%, and 5% for ^{24}Na, respectively. As the mass number of the product decreases, the contribution from π mesons increases. It is concluded that activation by π mesons is of growing importance in these high-energy shielding experiments.

Finally, it is clear that these peaks resulting from the experiments are influenced by the lack of shielding at the gaps. Although the effect of gaps was considered to be negligible when designing the hadron absorber, we found that even small gaps (~5 cm in diameter) may have a big impact on radiation shielding in the high-energy accelerator facility.

4. Conclusion

Two-dimensional distributions of the production rate behind the hadron absorber were obtained for pure aluminum and pure gold activation detectors. The distributions included some peaks caused by the gaps for arraignment and cooling of the absorber core. The differences between the side peaks by the gap and at the beam center were 2-5 times. For comparison with the experimental data, production rate was calculated by the PHITS code. From the calculation, it was found that the contributions to the production rate by π mesons become larger than those by other particles, except around the original target mass number. It was concluded that activation by π mesons and attenuation through π meson production is of growing importance in these high-energy shielding experiments. To continue this study, it was found that acquiring the cross section for π mesons is important.

Acknowledgment

This study is supported by a grand-aid of the Ministry of Education (KAKENHI 19360432, 21360473 and 23340172) in Japan. Fermilab is a U.S. Department of Energy laboratory operated under Contract DE-AC02-07CH 11359 by the Fermi Research Alliance, LLC.

References

[1] H. Nakashima, Y. Sakamoto, Y. Iwamoto et al., Experimental studies of shielding and irradiation effects at high-energy accelerator facilities, *Nucl. Technol.* 168 (2009), pp. 482-486.

[2] H. Hirayama and attenuation length sub-working group in Japan, Inter-comparison of the medium-energy neutron attenuation in iron and concrete (5), *Proc. of the Shielding Aspects of Accelerators, Target and Irradiation Facilities -SATIF7*, Sacavém, Portugal, 17-18 May, 2004, (2004), pp. 117-126.

[3] H. Nakashima, H. Takada, Y. Kasugai et al., Current status of the AGS spallation target experiment, *Proc. of the Shielding Aspects of Accelerators, Target and Irradiation Facilities –SATIF6*, SLAC, 10-12 Apr., 2002, (2002), p 27.

[4] N. Nakao, S. Taniguchi, S. H. Rokni, S. Roesler, M. Brugger, M. Hagiwara, H. Vincke, H. Khater and A. A. Prinz, Measurement of neutron energy spectra behind shielding of a 120 GeV/c hadron beam facility, *Nucl. Instr. Meth.* A562 (2006), pp. 950-953.

[5] K. Anderson, B. Bernstein, D. Boehnlein et al., *The NuMI Facility Technical Design Report*, Fermilab TM-2018, Fermi National Accelerator Laboratory, (1998).

[6] K. Niita, N. Matsuda, Y. Iwamoto, H. Iwase, T. Sato, H. Nakashima, Y. Sakamoto and L. Sihver, *PHITS: Particle and Heavy Ion Transport Code System, Version 2.23*, JAEA-Data/Code 2010-022, Japan Atomic Energy Agency, (2010).

[7] R. B. Firestone and V. S. Shirley, *Table of Isotopes, 8th edition*, Eds. John Wiley and Sons, Inc., New York, (1996).

[8] N. V. Mokhov, *Recent Mars15 Developments: Nuclide Inventory, DPA and Gas Production*, Fermilab-Conf-10-518-APC, Fermi National Accelerator Laboratory, (2010).

[9] F. L. Bronson, Validation of the accuracy of the LabSOCS software for mathematical efficiency calibration of Ge detectors for typically laboratory samples, *J. Radioanal. Nucl. Chem.* 255 (2003), p. 137.